The Astronomical Journal, 154:139 (10pp), 2017 October https://doi.org/10.3847/1538-3881/aa8307

Space Weathering of Super-Earths: Model Simulations of Exospheric Sodium Escape from 61 Virgo b

M. Yoneda[1,3], S. Berdyugina[1,3], and J. Kuhn[1,2]
[1] Kiepenheuer Institute for Solar Physics, Schöneckstraße 6, 79104 Freiburg im Breisgau, Germany
[2] Institute for Astronomy, University of Hawaii, 2680 Woodlawn Drive, Honolulu, HI 96822-1839, USA
Received 2017 January 31; revised 2017 July 21; accepted 2017 July 26; published 2017 September 8

Abstract

Rocky exoplanets are expected to be eroded by space weather in a similar way as in the solar system. In particular, Mercury is one of the dramatically eroded planets whose material continuously escapes into its exosphere and further into space. This escape is well traced by sodium atoms scattering sunlight. Due to solar wind impact, micrometeorite impacts, photo-stimulated desorption and thermal desorption, sodium atoms are released from surface regolith. Some of these released sodium atoms are escaping from Mercury's gravitational-sphere. They are dragged anti-Sun-ward and form a tail structure. We expect similar phenomena on exoplanets. The hot super-Earth 61 Vir b orbiting a G3V star at only 0.05 au may show a similar structure. Because of its small separation from the star, the sodium release mechanisms may be working more efficiently on hot super-Earths than on Mercury, although the strong gravitational force of Earth-sized or even more massive planets may be keeping sodium atoms from escaping from the planet. Here, we performed model simulations for Mercury (to verify our model) and 61 Vir b as a representative super-Earth. We have found that sodium atoms can escape from this exoplanet due to stellar wind sputtering and micrometeorite impacts, to form a sodium tail. However, in contrast to Mercury, the tail on this hot super-Earth is strongly aligned with the anti-starward direction because of higher light pressure. Our model suggests that 61 Vir b seems to have an exo-base atmosphere like that of Mercury.

Key words: planets and satellites: atmospheres – planets and satellites: surfaces

1. Introduction

Hot super-Earths of a few Earth masses and at short orbits around solar-type stars are a subclass of exoplanets discovered only a few years ago. They are often members of planetary systems with a few (sub-)Neptune class planets and debris disks. One of the brightest representatives is the nearby (only 8.5 pc away) G5 V star, 61 Vir, which hosts a planetary system of at least three planets within 0.5 au, among which a super-Earth, 61 Vir b, of $M \sin i = 5.1\,M_{\rm E}$ resides at only 0.05 au from the star (Vogt et al. 2010). As are a few others, this system is surrounded by a debris disk at 30–100 au, with the region inside 30 au possibly significantly depleted in planetesimals, and possibly having additional planets outside those already known (Wyatt et al. 2012). This disk imaged by the *Herschel Space Observatory* in the infrared is seen nearly edge-on, at 77°. Assuming that the known planetary system is approximately coplanar with the debris disk, 61 Vir b may have a mass of about $5.2\,M_{\rm E}$ and may still qualify as a super-Earth.

This class of objects is very interesting for studying space weathering and the evolution of planets. One example of planetary erosion by space weather could be a dramatically reduced mass of Mercury in the solar system, making its core look disproportionately large with respect to the mantle as compared to other rocky planets in the solar system (e.g., Orsini et al. 2014). Another dramatic example is the significant loss of the atmosphere on Mars (Lammera et al. 2003). In this paper, we use Mercury erosion as an example for modeling weathering processes in more extreme cases of hot super-Earths, in particular for 61 Vir b. Escaping surface material forms a so-called exosphere—a thin gaseous envelope that, in case of Mercury, the Moon, and other solar system objects, is best observed and traced via resonant scattering on sodium atoms. Modeling such a sodium exosphere on 61 Vir b using Mercury as a test example is the goal of this paper.

The existence of several atomic species in Mercury's exosphere has been found. Atomic oxygen, helium, and hydrogen were found by UV observations with the Mariner 10 spacecraft (Broadfoot et al. 1976). In addition to these atoms, sodium, potassium, and calcium atoms were found by ground-based observations (Potter & Morgan 1985, 1986; Bida et al. 2000). In particular, oxygen, helium, and sodium atoms have the largest column densities of the order of 10^{11} atoms cm^{-2}. The first detection of sodium atoms was by Potter & Morgan (1985). They observed sodium D-line emission (D1: 589.59 nm, D2: 588.99 nm). Sodium D-line emission is due to resonant scattering of solar radiation. The cross-section of this resonant scattering is large compared to the other species, so sodium atoms play an important role as a tracer of Mercury's exospheric particles.

Four processes, which are releasing sodium atoms from Mercury's surface regolith, have been proposed. They are solar wind ion sputtering (SWS), micrometeorite impact vaporization (MIV), photo-stimulated desorption (PSD), and thermal desorption (TD). Mercury has the smallest distance to the Sun among the planets in the solar system. This environment makes these mechanisms work efficiently. Mercury's exospheric sodium atoms are accelerated by solar radiation, and some of the sodium atoms are escaping from Mercury's gravitational-sphere and forming a tail structure (e.g., Baumgardner et al. 2008; Kameda et al. 2008).

Sodium has been found in other systems. For example, Charbonneau et al. (2002) found the sodium D-line absorption feature in HD209458b during its transit. However, this is a gas giant planet like Jupiter, and these sodium atoms are believed

[3] Visiting Researcher.

Table 1
Model Parameters of Mercury and 61 Virgo b, and Their Main Stars

	61 Vir b	Mercury
Masses of the planets (kg)	3.045×10^{25} (Valenti & Fischer 2005)	3.285×10^{23}
Radii of the planets (km)	10, 870	2,440
Distances from the main stars (au)	0.05 (Vogt et al. 2010)	0.39
Luminosities of the main stars ($L_\odot$)	0.8 (Valenti & Fischer 2005)	1
Spectral types of main stars	G5V (Cenarro et al. (2007))	G2V
Masses of main stars ($M_\odot$)	0.96 (Valenti & Fischer 2005)	1
Radiation fluxes from the main stars at 1 au (w cm^{-2})	1, 094 (=1, 368 $\times$ ($L/L_\odot$))	1, 368

to be in the planet's atmosphere. It can be said that this is different from exospheric sodium atmosphere like Mercury.

Vogt et al. (2010) pointed out that exoplanet 61 Vir b can be classified a super-Earth rather than a gas planet because of its small mass (5.1 M_E). Its star is a main sequence G-type, like the Sun. However, the orbital radius of this planet is 0.05 au. This distance is eight times smaller than that of Mercury. We can expect the four processes to be more efficient on 61 Vir b than on Mercury. On the other hand, the mass of this planet is 100 times greater than that of Mercury. This can suppress the escape of exospheric atoms from the planet. We performed model simulations for exospheric sodium atoms both on 61 Vir b and Mercury to see whether 61 Vir b has an exo-base surface similar to Mercury or if its mass allows this planet to keep its atmosphere like Venus. Mars is not perhaps a good example here as it lost a lot of its atmosphere. This planet is not the only (potential) super-Earth ever found, and its transit cannot be seen from the Earth. However, parameters about this planet and its star are better known compared to the other super-Earth candidates. Furthermore, the star is G-type in the main sequence. So we can infer the unknown parameters for 61 Vir b from those for the Sun.

2. Model Simulations

The model deals with the four mechanisms separately (SWS, MIV, PSD, and TD). In our model, MIV works in both hemispheres, but the other three work only in the day-side hemisphere. Our model is a Monte-Carlo simulation in which initial positions and velocity vectors of packets that include sodium atoms are given randomly. Numbers of sodium atoms decrease with a timescale of ionization. This timescale is discussed later. The small orbital radius of 61 Vir b indicates that its rotation is probably synchronized with its revolution. Also, Mercury's rotation is as slow as 58.5 days. Therefore, velocities given by the planets' rotation are probably low and not taken into account in our model. This means the initial velocity is a combination of the vector of the orbital motion and that given by releasing mechanism (SWS, MIV, PSD, and TD). Parameters of these two planets are summarized in Table 1.

The size of 61 Vir b is unknown, as its transit has never been observed. Here, we assume that this planet has the same mass density as that of the Earth. This assumption gives a radius of 10,870 km, as shown in Table 1.

2.1. Solar Wind Ion Sputtering: SWS

Wiens & Burnett (1997) performed experiments in which they measured velocity distributions of sodium atoms that were generated by ion beams into surfaces covered by Na_2SO_4 molecules. The velocities they found by the experiment matched Sigmund–Thompson distributions that can be described as,

$$F(v) = \frac{1}{D}\frac{v^2}{v^2 + {v_b}^2}\left(1 - \frac{v^2 + {v_b}^2}{{v_M}^2}\right) \quad (1)$$

$$v_M = \frac{2M}{M + m} v_R, \quad (2)$$

where $F(v)$ is the velocity distribution function, D is a factor for normalization, m and M are the masses of a sodium atom and incident ion, respectively, v is the velocity of the sodium atoms, v_b is the binding energy of the sodium atoms with the surface regolith converted to velocity so the actual binding energy is $\frac{1}{2}m{v_b}^2$, and v_M is the velocity of the protons in the stellar wind. Assuming an energy of 1 keV, which is a typical proton energy in the solar wind, v_M can be obtained as 36.7 km s^{-1}. Figure 1 shows the feature produced by this velocity distribution function. With this distribution function, 3% of the atoms can exceed 5 km s^{-1}, although the most probable speed is $\sim$1 km s^{-1}.

The SWS on Mercury is believed to occur only in the polar regions, as Mercury has an intrinsic dipole magnetic field. Kameda et al. (2008) and Schleicher et al. (2004) showed the sodium D-line emissions enhanced above Mercury's polar regions based on their ground-based observations. However, we do not know whether 61 Vir b has its own magnetic field. In our model, the magnetic fields of the planets are not taken into account. This means SWS occurs only on day-side hemispheres, and the number of sodium atoms released from a unit surface area is proportional to the cosine of the solar zenith. In an equation, it can be expressed as

$$\Phi_{SWS} = R_{SWS} \cos\chi, \quad (3)$$

where ϕ_{SWS} is the number of sodium atoms released from a unit surface, R_{SWS} is the number of sodium atoms released from a unit surface but at the sub-solar point, and χ is the solar zenith angle. McGrath et al. (1986) estimated the flux of sodium atoms due to SWS as 2.0×10^7–2.0×10^8 cm^{-2} s^{-1} at most. We adopt a number of 2.0×10^8 cm^{-2} s^{-1} for R_0 on Mercury. Wood et al. (2005) argued that the energy and mass fluxes of stellar wind of 61 Vir b are 30% of those of Sun. This means the average proton energy (velocity) in the stellar wind of 61 Vir b is 30% of the Sun. We can use the same distribution function for 61 Vir b as Equation (1) and the first panel in Figure 1. However, a proton flux at the sub-main star point is 17 times larger than that of Mercury if the proton number density in the stellar wind is proportional to the inverse square

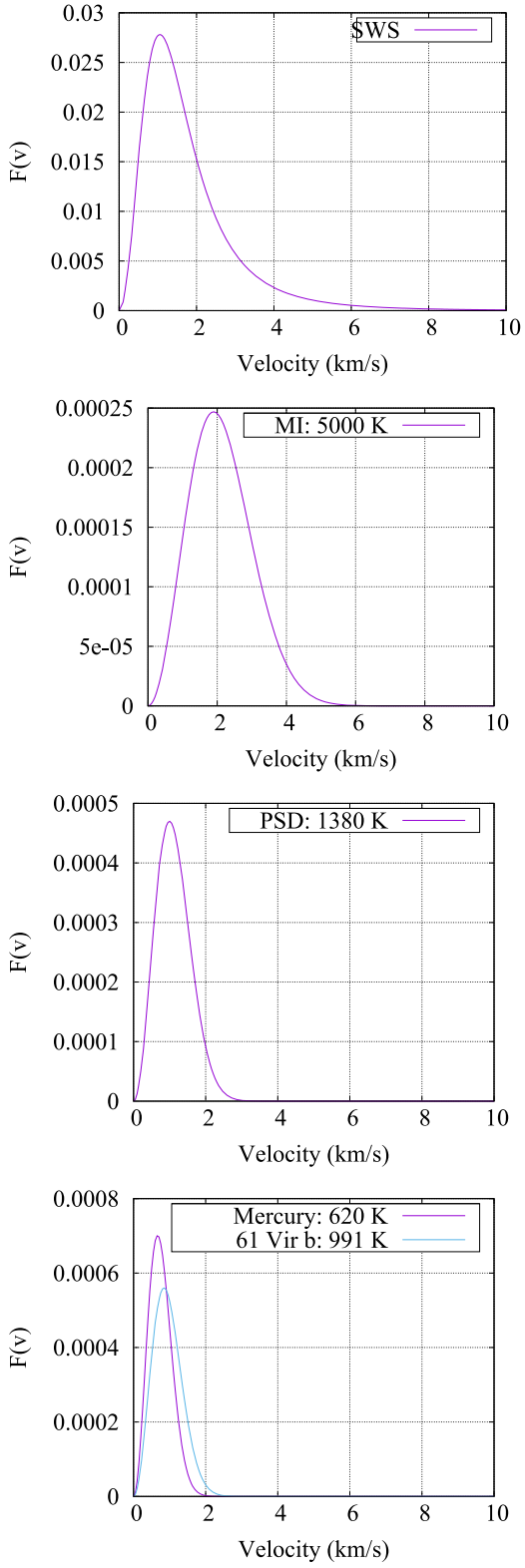

Figure 1. The curves show velocity distributions for solar wind sputtering (top), micrometeorite impacts (2nd), photo-stimulated desorption (3rd), and thermal desorption (bottom). The velocity distribution by SWS shows a Sigmund–Thompson distribution, but the other three are well-reproduced by the Maxwellian.

of the distance from the main star $\left(0.3 \times \frac{0.39\ \mathrm{au}^2}{0.05\ \mathrm{au}} = 17\right)$. In our model, R_0 is 2.0×10^8 cm^{-2} s^{-1} for Mercury and 3.4×10^9 cm^{-2} s^{-1} for 61 Vir b, respectively.

2.2. Micrometeorite Impact: MI

Due to the impact by micrometeorites on the planet's surface, vaporization of the surface regolith occurs. Sugita et al. (1997) performed collision experiments and measured temperatures in sodium gas, which was vaporized by the collisions. They derived sodium gas temperatures of 6000 and 4200 K with incident angles of 60° and 30°, respectively. In this model, a velocity distribution function of sodium atoms due to MI is given as the Maxwell function with a temperature of 5000 K both for Mercury and 61 Vir b. This is a rough average between 6000 and 4200 K. Killen et al. (2004) showed that the number flux of sodium atoms averaged all over the surface is 3.0×10^7 cm^{-2} s^{-1}. In our model, this flux is adopted uniformly all over the surface for both planets.

2.3. Photo-stimulated Desorption: PSD

The PSD was first proposed by McGrath et al. (1986) as one of main sources of Mercury's exospheric atmosphere. In this process, UV photons from the Sun strike surface regolith and release atoms in it. Yakshinskiy & Madey (1999) performed experiments in which electron beams were hitting SiO_2 films with depositions of sodium atoms. The SiO films simulated the lunar surface and the electron energy was 200 eV. A Maxwellian function with a temperature of 1380 K fitted speeds of the released sodium atoms in their experiments. Killen et al. (2004) showed number of sodium atoms at the subsolar point on Mercury is (2.5–6.0) $\times 10^7$ cm^{-2} s^{-1}. Because the number of sodium atoms released from unit area-of-surface per unit time is proportional to the solar zenith angle of that point, it can be expressed as a function of χ as below,

$$\Phi_{\mathrm{PSD}} = R_{\mathrm{PSD}} \cos\chi, \tag{4}$$

$$R_{\mathrm{PSD}} = F_{\mathrm{ph}} Q \sigma f_{\mathrm{Na}}, \tag{5}$$

where Φ_{PSD} is the source rate at the stellar zenith angle of χ, F_{ph} is the stellar UV photon fluxes at the planets' orbits that cause photo desorption of atoms in the surface regoliths, Q is the cross-section of photo desorption, and σ is the number density of atoms that form at the surface regolith per unit surface area, and f_{Na} is the ratio of sodium atoms in the surface regoliths. We do not know the exact UV flux of 61 Vir, so we make an assumption that the UV flux of this star is proportional to its luminosity. The luminosity of 61 Vir is 0.8 $L_\odot$ (Vogt et al. 2010), and this implies that photon flux at 61 Vir b is 50 times larger than that of Mercury $\left(0.8 \times \left(\frac{0.39\ \mathrm{au}}{0.05\ \mathrm{au}}\right)^2 = 50\right)$. In our model, we assume that parameters such as Q, σ, and f_{Na} are the same between the two planets. The value for R_{PSD} on Mercury is given as 4.0×10^7 cm^{-2} s^{-1} based on Killen et al. (2004), and 2.0×10^9 cm^{-2} s^{-1} for 61 Vir b, which is 50 times of that of Mercury. The speed distribution function is Maxwellian with a temperature of 1380 K, that gives a most probable speed of 1 km s^{-1}.

2.4. Thermal Desorption: TD

Sodium atoms are released from the surface of the planets when their thermal energies exceed binding energies of molecules that include the sodium atoms. Yakshinskiy et al. (2000) performed an experiment in which they observed the behavior of sodium atoms attached onto thin SiO_2 films, and

they found sodium atoms were released when the temperature was higher than 400 K. The velocities of sodium atoms due to TD are given by the Maxwellian function with local temperatures. The local temperature can be derived with a function as below,

$$T = \left(\frac{F\cos\chi(1-A)}{4\sigma_0}\right)^{1/4}, \quad (6)$$

were T is the temperature, F is the radiation flux from the main star, A is the albedo of the planet, and σ_0 is the Stephan-Boltzmann constant. The radiation flux F can be expressed as,

$$F = S\frac{L}{L_\odot}\frac{1}{r^2}, \quad (7)$$

where S is the solar constant and its exact number is 1368 W m^{-2}, L is the luminosity of the main star, r is the distance from the main star in a unit of au. We assumed an albedo of 0.5 for 61 Vir b, and that gives temperatures at sub-stellar points as 991 K on 61 Vir b. However, for Mercury, we adopted a different function proposed by Butler (1997) that reproduces surface temperature, which is expressed as,

$$T = 220 \times \left(\frac{0.306}{r}\right)^2 + 480 \times (\cos\chi)^{1/4}. \quad (8)$$

This is a better approximation for slow rotators like Mercury and the Moon. Killen et al. (2004) and Leblanc & Johnson (2003) adopted the same function in their simulations.

Based on results by Yakshinskiy et al. (2000), a number of sodium atoms released by TD from a unit surface per unit time is given as below,

$$\Phi_{\rm TD} = \nu_s \sigma f_{\rm Na} \exp\left(-\frac{U}{k_b T}\right), \quad (9)$$

ν_s is the oscillation frequency in the solid surface, and U is the binding energy of sodium atoms in the surface regolith. This function is used in the model for the planets. The oscillation frequency ν is given as 10^{13} Hz as shown by Hunten et al. (1988). We do not know the exact values for ν_s, σ, $f_{\rm Na}$, and U on the both planets. Heiken et al. (1991) showed these values on lunar surface as $\sigma = 7.5 \times 10^{14}$ cm^{-2}, $f_{\rm Na} = 0.005$, and $U = 1.85$ eV. These values are adopted in our models for the planets.

2.5. Equation of Motion

Sodium atoms feel the gravitational forces of the star, the planet, and radiation pressure from the star. Therefore, an equation of motion of the sodium atoms can be expressed as below,

$$\frac{\partial^2 \boldsymbol{r}}{\partial t^2} = -\frac{GM_S}{r^3}\boldsymbol{r} - \frac{GM_P}{(r-r_P)^3}(\boldsymbol{r}-\boldsymbol{r}_P) + \boldsymbol{b}, \quad (10)$$

where $\boldsymbol{r}$ and $\boldsymbol{r}_P$ are the vectors that show positions of the sodium atoms and planets, respectively, G is the gravitational constant, M_S and M_P are masses of stars and planets, respectively. Smyth (1979) showed that the radiation pressure on the sodium atoms from the stars, which is described as $\boldsymbol{b}$, can be derived as,

$$b = \Sigma_i \frac{h\nu_i}{mc} J_i \quad (11)$$

where h is the Planck constant, m is the electrons mass, and c is the light constant. Integer values of $i = 1$ and $i = 2$ mean sodium D1 and D2, respectively. Therefore, ν_1 and ν_2 are frequencies at sodium D1 and D2 wavelengths, and J_1 and J_2 are numbers of photons that sodium atoms absorb at the D1 and D2 wavelengths in a unit time. Here, J_i can be expressed as,

$$J_i = \sigma_i \gamma(\lambda)\frac{\pi F}{r^2}\frac{1}{\nu_i}, \quad (12)$$

$$\sigma_i = \frac{\pi e^2}{m_e c} f_i, \quad (13)$$

where σ_i is the cross-section of sodium atoms for resonant scattering at D1 and D2 wavelengths, $\gamma_i(\lambda_i)$ is the ratio of fluxes from the main stars at Doppler shifted D-line wavelengths to the continuum fluxes out of the Fraunhofer absorption wavelengths, F is the radiation flux from the main stars at 1 au, r is the distance of the sodium atoms from the main star, e is the electron charge, and f_i is the oscillation strength factors ($f_1 = 0.327$ and $f_2 = 0.655$). The equation of motion is solved numerically using the fourth order Runge–Kutta method in the model. The solar flux, shown as γ in Equation (12), is given as a function of the wavelength as,

$$\gamma(\lambda) = 1 - a_1 \exp\left(-\frac{|\lambda-\lambda_1)|}{b_1}\right) - a_2 \exp\left(-\frac{|\lambda-\lambda_2)|}{b_2}\right), \quad (14)$$

$$\lambda = \frac{c-v}{c}\lambda_i, \quad (15)$$

where v is the speed of sodium atoms with the main star, λ_1 and λ_2 are the wavelengths at the sodium D1 and D2 line, respectively, a_1, a_2, b_1, and b_2 are the fitting parameters. The function $\gamma(\lambda)$ is obtained by fitting the function to the solar data from FTS NSO Solar spectral atlases.[4] This data and fitting function are shown in Figure 2.

The D-line brightness with a unit of Rayleigh/str can be described as,

$$I_i = \frac{10^{-6} J_i N}{4\pi}, \quad (16)$$

where N is the column density of the sodium atoms in a unit of atoms cm^{-2}, $i = 1$ for D1 and $i = 2$ for D2 line.

2.6. Loss Process of Sodium Atoms

In the model, sodium atoms colliding with the planets' surfaces are treated as lost particles. Another loss process is ionization. The ionization is caused by the photon impacts from the main stars or collision with the stellar wind particles. Cremonese et al. (1997) derived a lifetime of neutral sodium atoms based on their observational results of sodium emissions in the tail of the comet Hale-Bopp as 1.7×10^5 s. Adopting their results and assuming that the lifetime is proportional to the inverse of the luminosities of stars, sodium lifetimes in our

[4] ftp://nispdata.nso.edu/pub/atlas/

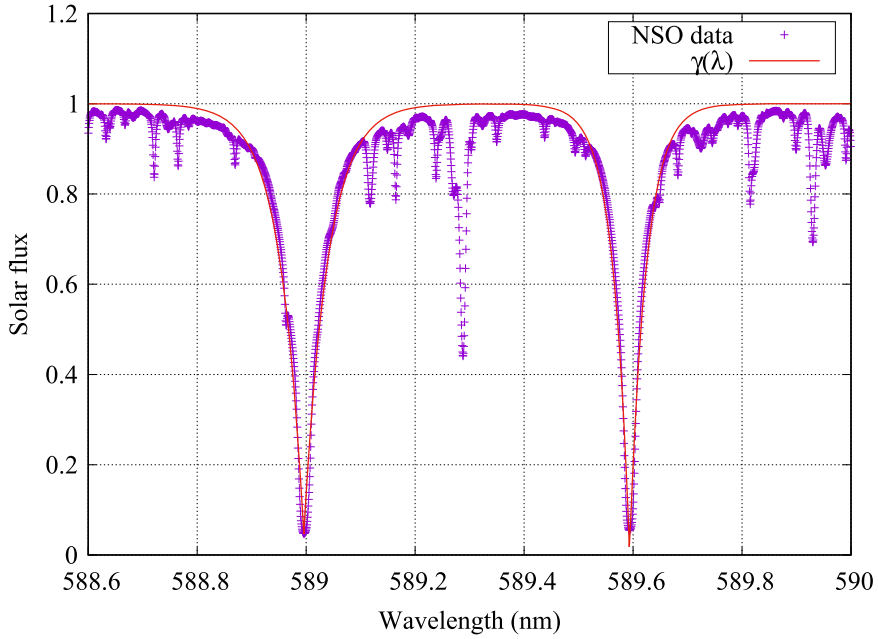

Figure 2. The observed solar flux spectrum (FTS NSO Solar spectral atlases ftp://nispdata.nso.edu/pub/atlas/) with the sodium D1 and D2 lines (symbols) shows the fitting function $\gamma(\lambda)$. Each value is normalized by the solar continuum level.

model are given as,

$$\tau = 1.7 \times 10^5 \frac{L_\odot}{L} \frac{1}{r^2}, \quad (17)$$

where τ is the lifetime of the neutral sodium atoms (s) at the distance r from the main stars (au).

3. Results

3.1. Mercury

The model calculation results are shown in Figure 3 as column densities of sodium atoms and D1 + D2 brightness. As suggested by past studies (e.g., Killen et al. 2004), we can see that sodium atoms produced by PSD and TD tend to stay near Mercury's surface, while those by SWS and MI are escaping from the planet and form a tail structure in the anti-solar direction. With PSD, we cannot see any significant sodium escape, but some of the sodium atoms are flying to the night-side hemisphere from the day-side, while the sodium atoms by TD can be seen only in the day-side hemisphere. This is because initial velocity given by PSD is larger than that of TD. For PSD, the photon energy is assumed to be 200 eV. This energy corresponds to a wavelength in X-ray rather than UV, so the actual velocity given by PSD should be smaller than that given in this model. It can be said that PSD and TD do not contribute to the exospheric sodium escape. In Figure 4, more detailed values in the column density and D1 + D2 are shown as a function of distance from Mercury. The largest brightness is obtained on Mercury's Sun-facing surface as $\sim 10^6$ (Rayleighs/str), and that at 8 Mercury's radii is $\sim 10^{3.5}$ (Rayleighs/str). These are consistent with observational results by Potter et al. (2002). They performed observations of sodium emissions using the MacMath-Pierce solar telescope whose aperture was 1.6 m, and obtained the D-line brightness within 20 Mercury radii. The sodium tail observed by Potter et al. (2002) is well-reproduced in our model. The consistency between their observational results and our model results suggests that the model is working properly.

3.2. 61 Virgo b

The simulation results for 61 Vir b are shown in Figure 5. Sodium atoms released by SWS and MI are escaping from the planet's gravitational-sphere and form a sodium tail in the opposite direction of the main star. This tendency is the same as that of Mercury except the Mercury tail is not so clearly defined. The main source of sodium atoms in the day-side hemisphere is from TD. The sodium atoms in the night-side hemisphere on the planet's surface are mainly from MI, as MI is the only mechanism that works over the surface uniformly.

4. Discussion

Both planets show escape of sodium atoms by SWS and MI. However, there are several differences in detail. While sodium atoms escaping from 61 Vir b have a sharp tail-like structure, those escaping from Mercury look diffuse. The sodium clouds around Mercury are, to some extent, even Sun-ward facing. This is because the radiation pressure and gravitational force at the surface of 61 b are stronger than those at Mercury by 46 and 4.5 times, respectively. The star 61 Vir b is G-type in the main sequence, as is the Sun. Therefore, the small distance directly reflects the strong radiation pressure. Not only does this small radius increase the radiation pressure, it also works to increasing the source rates of SWS, PSD, and TD. Actually, those of this planet show greater values both in the column density and brightness compared to those of Mercury. Although TD on 61 Vir b produces faster sodium atoms than TD on Mercury, it does not cause the escape of sodium atoms because of its strong gravitational force. Because of the greater gravitational force, escaping sodium atoms from 61 Vir b are focused on the star–planet line, which is in the shadow of the planet where the atoms have no photons to scatter. Thus, distributions of the number density and brightness are different,

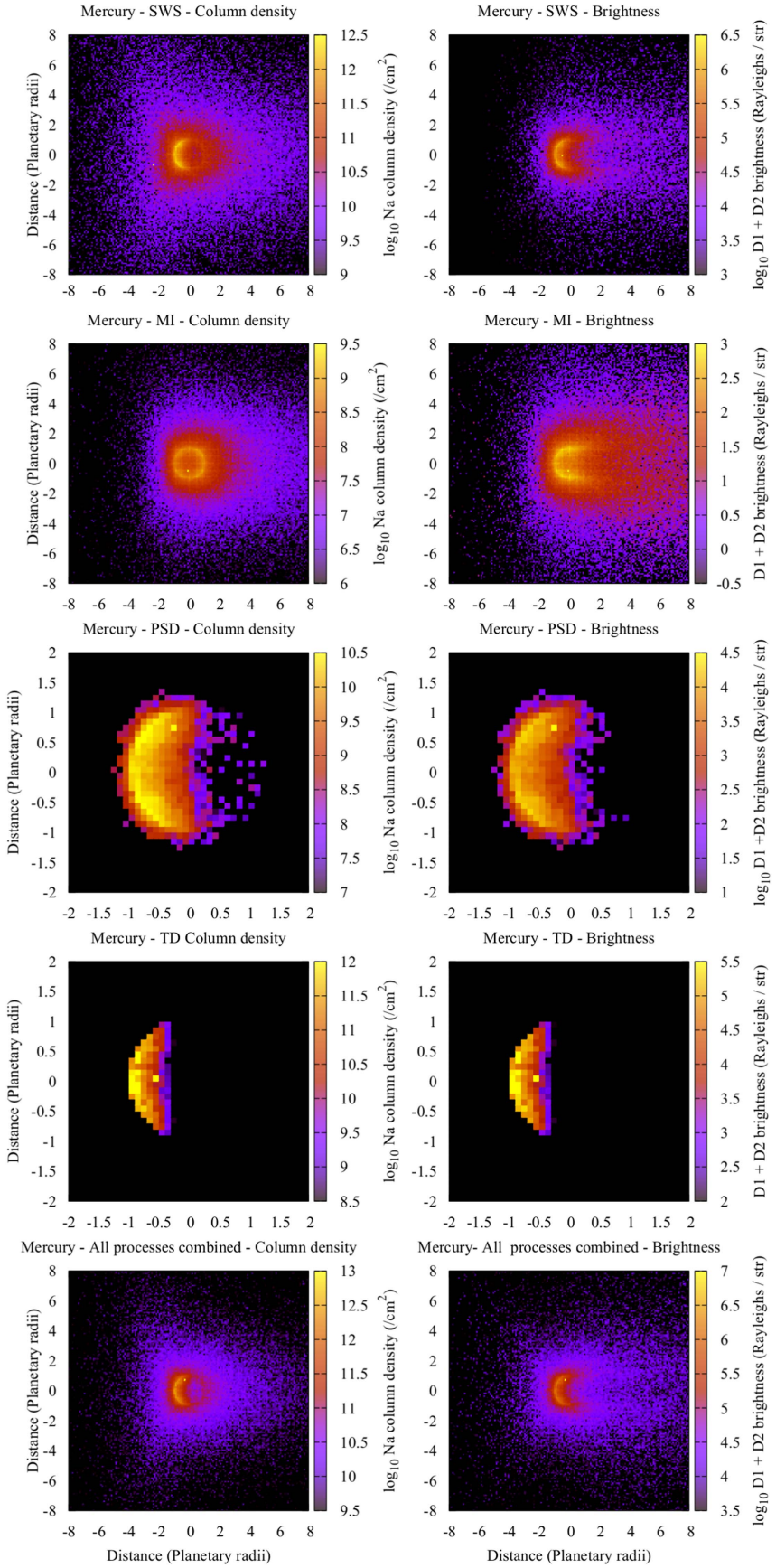

Figure 3. Model results of column densities of sodium atoms (left panels) and sodium D-line brightness (right panels) around Mercury. Calculation results are shown separately by releasing processes (top: SWS, second: MI, third: PSD, fourth: TD, bottom: all processes are combined). The $x+$ direction corresponds to anti-Sun-ward direction, and $y+$ corresponds to the northern orbital axis. The spatial scale is within 2 planetary radii for TD and PSD, but 8 radii for SWS and MI, as they make structures outside of the planet. Also, the color scale is different for each.

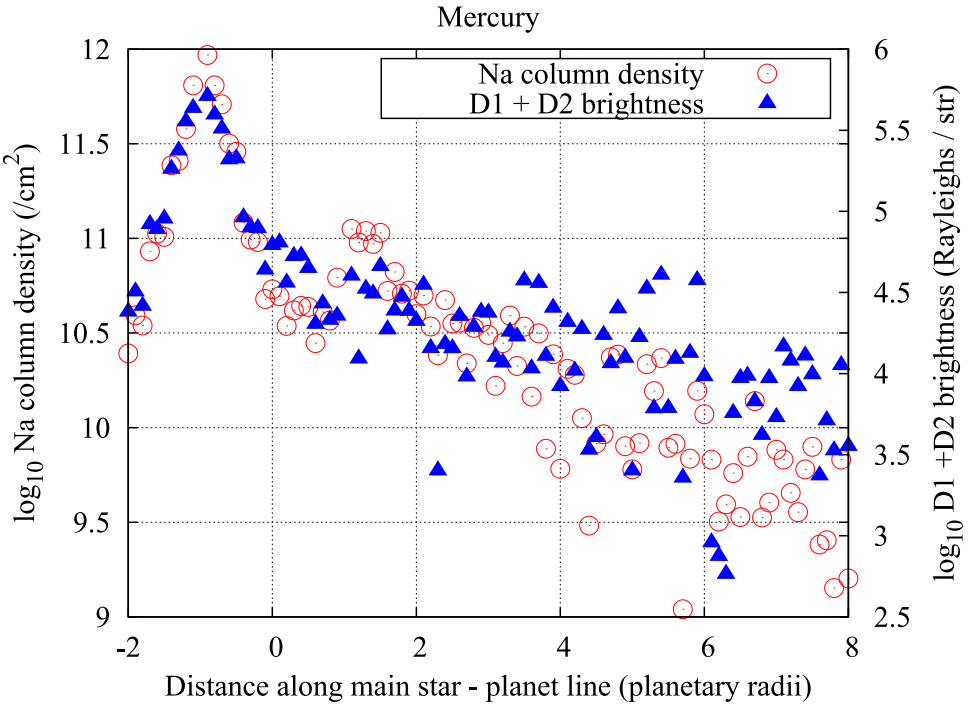

Figure 4. Model results that show column density and sodium D1 + D2 brightness as functions of distance from Mercury along the Sun–Mercury axis.

as seen in the bottom panel of Figure 5. As seen in Figures 4 and 6, the sodium atom number density and brightness decrease with the increase of distance from the planets. This tendency looks more significant with 61 Vir b than Mercury. However, the distances in these panels are normalized by planetary radii. Therefore, the gap between these planets is not necessarily significant.

Before neutral escape occurs, ionospheric escape is expected. For example, the solar wind does not strike Mars's surface, but it interacts with Mars's ionosphere. The ionospheric plasma can be picked up and accelerated by the magnetic fields in the solar wind. A similar ionospheric escape is expected to occur on exoplanets like on Mars (e.g., Lammera et al. 2003). After losing ionospheric atmosphere, planets' surfaces finally begin to interact with the stellar winds directly. Because of the small orbital distance of 61 Vir b to its star, the planet's ionosphere may have been displaced already. This means the surface of 61 Vir b could be exposed to the stellar wind directly, and its exospheric atmosphere is escaping as our model simulations show. Another possibility is that exospheric sodium atoms have been exhausted because of the strong interaction with the star, although micrometeorites may contribute to re-supply to the planet's surface. We cannot conclude that the sodium escape shown in our model simulations is happening on 61 Vir b now, but it should have happened during the atmospheric evolution of this planet.

Because the orbital period of 61 Vir b is only 4.15 days, it can be expected that the sodium tail of the exoplanet shows a certain curvature. However, this curvature is not so significant as long as the focusing regions are close to the planet, as seen in the left panel of Figure 7. On the other hand, we can see a significant asymmetry in the exospheric sodium structure from the view of the star–planet direction, as shown in the right panel of Figure 7. This asymmetry is due to the fast orbital motion. In fact, transit observation of Mercury by Schleicher et al. (2004) did not show such a significant asymmetry.

This planetary system does not show its transit to the solar system because of its large inclination angle. However, absorption spectra from the sodium atmosphere in the planet's exosphere are still an interesting issue. We estimated the level of absorption feature by the exospheric sodium atoms around the sodium D2 line with the assumption that we can observe its transit from the Earth, as shown in Figure 8. We assumed that the spectral resolution is 10^5 (=5.59×10^{-3} nm) and the planet is on the center of the star's disk. Cox (2000) showed that the solar limb darkening can be expressed as,

$$\frac{I'(d)}{I'(0)} = \sum_{i=0}^{\infty} b_i (1 - d^2)^{0.5i}, \tag{18}$$

where d is the distance from the star's disk center in a unit of stellar radius, $I'(d)$ is the surface brightness of the disk at a distance of d from the disk center, and b_i is the coefficient for the ith order. The same expression is used for 61 Vir in this study. The maximum order used in this simulation is $i = 2$, and the coefficients are $b_0 = 0.3$, $b_1 = 0.93$, and $b_3 = 0.23$. This coefficient set is for a wavelength of 550 nm. Even with this high spectral resolution, the largest absorption is only 3×10^{-6}, so it can be said that observation of absorption by sodium atoms in super-Earths' exospheres is difficult but may be possible using spectropolarimetry techniques. Sodium D2 emission can show linear polarization depending on the phase angle. Ariste et al. (2012) observed polarization in sodium D2 emission in Mercury's exosphere; however, observed polarization was smaller than expected. They concluded too much optical depth decreased the polarization. So spectropolarimetry is one method that can be used to observe super-Earths' sodium exospheres, but we cannot be very optimistic. An interesting feature shown in the spectrum is that the absorption has a certain extent toward shorter wavelength, particularly in a range of 589.56–589.58 nm. This is caused by the sodium

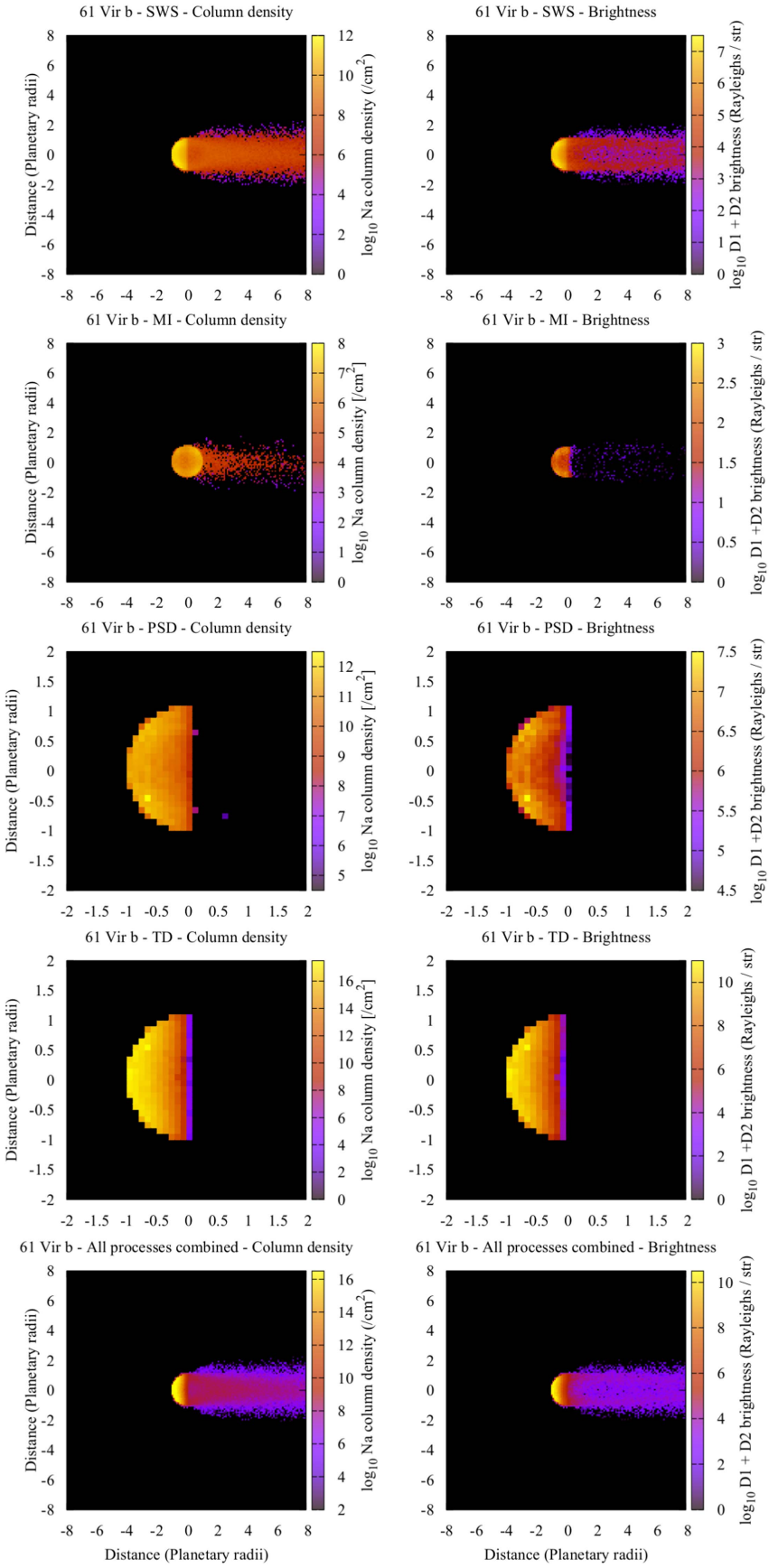

Figure 5. Model results shown in the same format as Figure 3, but for 61 Vir b.

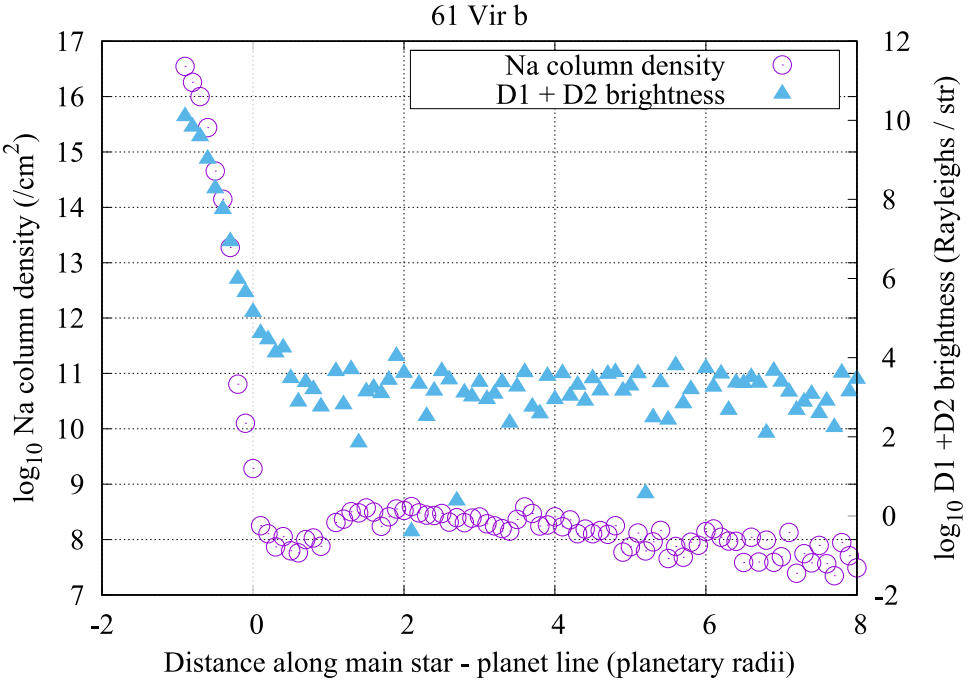

Figure 6. Model results shown in the same format as Figure 4, but for 61 Vir b.

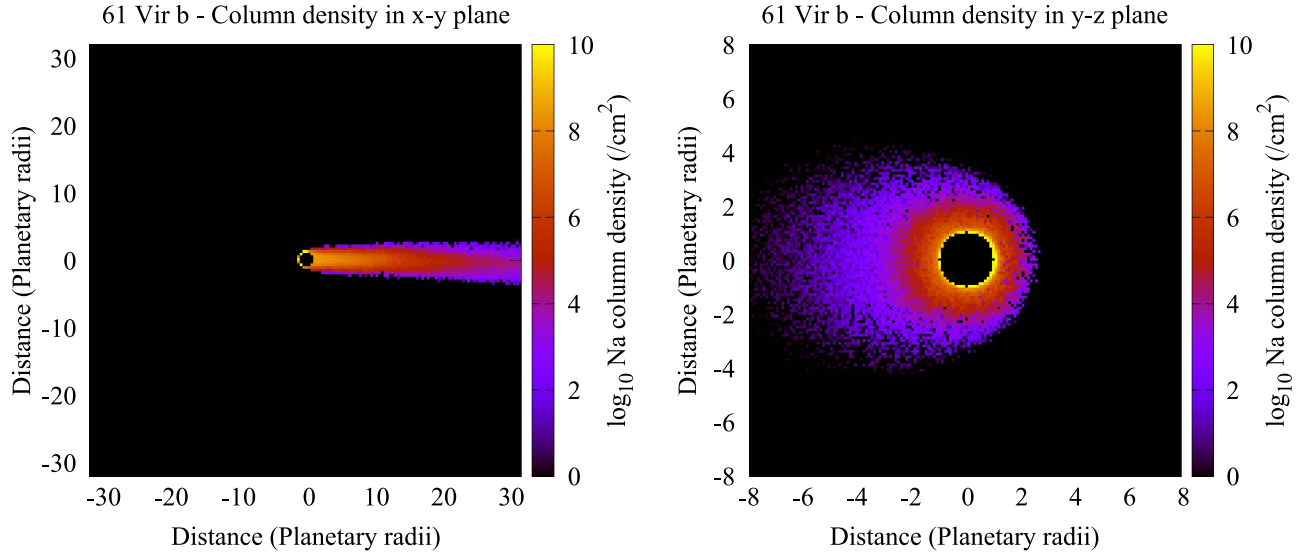

Figure 7. Model results of column densities of sodium atoms around 61 Vir b. The left panel shows it in its orbital plane, so the $y+$ direction corresponds to the planet's orbital velocity, and the $x+$ corresponds to anti-star direction. In the right panel, the $x+$ corresponds to the planet's orbital velocity, and the y-axis is perpendicular to the planet's orbital plane. Column densities on the disk are not shown to focus on ambient structures around the planet.

atoms in the tail structure. These particles in the tail are escaping from the planet's gravitational-sphere with velocities toward the observer, and this results in the absorption at shorter wavelengths.

5. Summary

We have performed model simulations to reproduce the escape of sodium atoms from Mercury and the exoplanet 61 Vir b. The model results for Mercury are consistent with past observational results, and this indicates that the model works properly. With the assumption that the composition of the surface regolith on 61 Vir b is similar to Mercury, we obtain the parameters specified in the model. The model results show that Stellar Wind Sputtering and Micrometeorite Impacts liberate sodium atoms both on Mercury and 61 Vir b, but Thermal Desorption does not. On Mercury, Photo-Stimulated Desorption works in the transportation of sodium atoms from the day-side hemisphere to the night-side, but this effect is not significant on 61 Vir b. The escaping sodium atoms from 61 Vir b showed a tail-like structure similar to Mercury, but its shape was less diffuse than that of Mercury because of the difference in radiation pressures from the central stars. We can conclude that exospheric sodium atoms can escape from this exoplanet despite its strong gravitational force. The sodium is not the only species that could be controlled by the radiation pressure, and exospheric escape can work for other

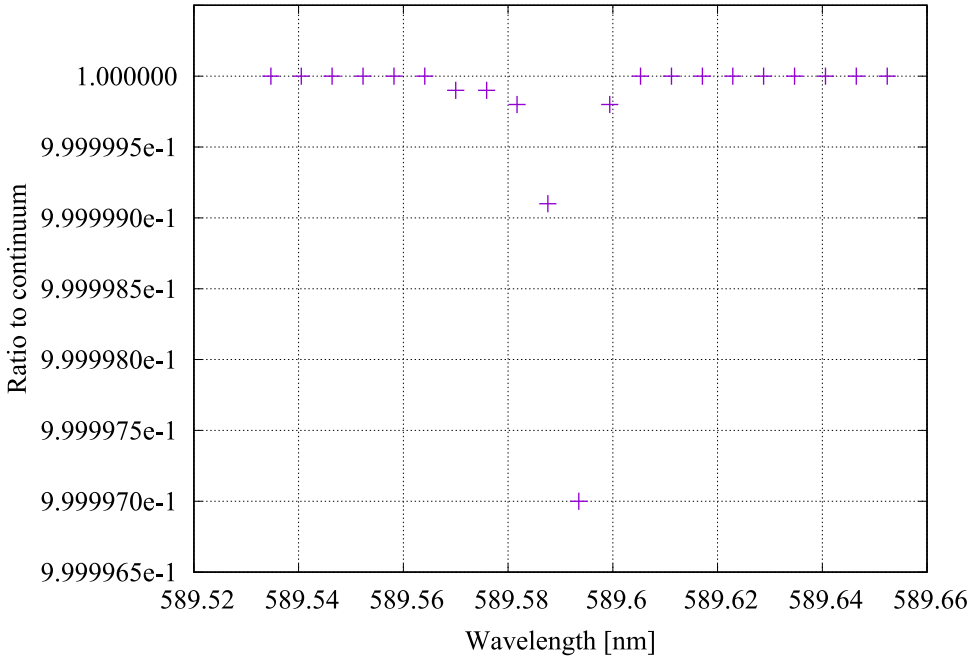

Figure 8. Spectrum caused by absorption of sodium atoms in the exosphere around the wavelength of sodium D2 line. The absorption strength is shown as a ratio to the continuum level. Here, we assume that the spectral power is 10^5 ($=5.59 \times 10^{-3}$ nm) and the planet is on the center of the star's disk.

atoms. Our work indicates that super-Earths that have small orbital radii and whose main stars are G-type in the main sequence or heavier have exo-base surfaces and do not have collisional atmospheres. On the other hand, some super-Earths found so far have main sequence M-type stars. Luminosities of these stars are smaller than G-type stars by three orders of magnitude. This means radiation pressure is also smaller by the same order. When we performed a model simulation for 61 Vir b, but with a radiation pressure that was smaller than the actual pressure by 1000 times, we did not see any atmospheric escape. We expect that atmospheric escape from super-Earths is strongly dependent on the spectral types of main stars.

This work has been supported by the ERC Advanced Grant HotMol. The authors appreciate practical advice from Drs. H. Misawa, Tohoku University, and M. Yagi, Riken, Japan. The authors thank the anonymous reviewer and editor Dr. Michael Endl for their advice, which improved this study.

ORCID iDs

M. Yoneda https://orcid.org/0000-0002-7773-7612

References

Ariste, A. L., Leblanc, F., Casini, R., et al. 2012, Icar, 220, 1104
Baumgardner, J., Wilson, J., & Mendillo 2008, GeoRL, 35, 3201
Bida, T. A., Killen, R. M., & Morgan, T. H. 2000, Natur, 404, 159
Broadfoot, A. L., Shemansky, D. E., & Kumar, S. 1976, GeoRL, 3, 577
Butler, B. J. 1997, JGR, 102, 19283
Cenarro, A. J., Peletier, R. F., Sànchez-Blàzquez, P., et al. 2007, MNRAS, 374, 664
Charbonneau, D., Brown, T. M., Noyes, R. W., & Gilliland, R. L. 2002, ApJ, 568, 377
Cox, A. N. 2000, in Allen's Astrophysical Quantities, ed. A. N. Cox (4th ed., New York: AIP, Springer)
Cremonese, G., Boehnhardt, H., Crovisier, J., et al. 1997, ApJL, 490, 199
Heiken, G., Vaniman, D., & French, B. M. 1991, Lunar sourcebook (Cambridge Univ. Press: New York), 736
Hunten, D. M., Morgan, T. H., & Shemansky, D. E. 1988, in Mercury, ed. F. Vilas, C. R. Chapman, & M. S. Matthews (Tucson, AZ: Univ. Arizona Press), 562
Kameda, S., Kagitani, M., Okano, S., Yoshikawa, I., & Ono, J. 2008, AdSpR, 41, 1381
Killen, R. M., Sarantos, M., Potter, A. E., & Reiff, P. 2004, Icar, 171, 1
Lammera, H., Lichteneggerb, H. I. M., Kolba, C., et al. 2003, Icar, 165, 9
Leblanc, F., & Johnson, R. E. 2003, Icar, 164, 261
McGrath, M. A., Johnson, R. E., & Lanzerotti, L. J. 1986, Natur, 323, 694
Orsini, S., Mangano, V., Mura, A., et al. 2014, Icar, 239, 281
Potter, A. E., & Morgan, T. H. 1985, Sci, 229, 651
Potter, A. E., & Morgan, T. H. 1986, Icar, 67, 336
Potter, A. E., Killen, R. M., & Morgan, T. H. 2002, M&PS, 37, 1165
Schleicher, H., Wiedemann, G., Wöhl, H., Berkefeld, T., & Soltau, D. 2004, A&A, 425, 1119
Smyth, W. H. 1979, ApJ, 234, 1148
Sugita, S., Schultz, P. H., & Adams, M. A. 1997, in 28th Annual Lunar and Planetary Science Conf., In Situ Temperature Measurements of Impact-induced Vapor Clouds with a Spectroscopic Method (Houston, TX: LPI), 1393
Takeda, G., Ford, E. B., Sills, A., et al. 2007, ApJS, 168, 297
Valenti, J. A., & Fischer, D. A. 2005, ApJS, 159, 141
Vogt, S. S., Wittenmyer, R. A., Butler, R. P., et al. 2010, ApJ, 708, 1366
Wiens, R. C., & Burnett, D. S. 1997, Icar, 128, 386
Wood, B. E., Müller, H.-R., Zank, G. P., Linsky, J. L., & Redfield, S. 2005, ApJL, 628, L143
Wyatt, M. C., Kennedy, G., Sibthorpe, B., et al. 2012, MNRAS, 424, 1206
Yakshinskiy, B. V., & Madey, T. E. 1999, Natur, 400, 642
Yakshinskiy, B. V., Madey, T. E., & Ageev, V. N. 2000, Surface Rev. Lett., 7, 75